CHITIN NANOFIBRES AS REINFORCEMENT FOR HYDROXYAPATITE-BASED COMPOSITE PREPARATION

Tomasz Machałowski[1,*], Mikołaj Kozłowski[2], Agnieszka Kołodziejczak-Radzimska[1], Jarosław Jakubowicz[2], Teofil Jesionowski[1]

[1] Institute of Chemical Technology and Engineering, Faculty of Chemical Technology, Poznan University of Technology, Berdychowo 4, 61-131 Poznan, Poland
[2] Institute of Materials Science and Engineering, Faculty of Materials Engineering and Technical Physics, Jana Pawla II 24, 61-138 Poznan, Poland

**corresponding author: tomasz.g.machalowski@doctorate.put.poznan.pl*

Abstract

The development and improvement of chitin applications have drawn special attention from the global scientific community due to their extraordinary features and abundance. In this study, β-chitin nanofibres were obtained using the ultrasonication treatment method. Then, hydroxyapatite/nanochitin (HAp/NCh) composites were prepared at different maturation times. In this case, mixtures of various amounts of β-chitin nanofibres (1%, 2%, and 5%) were added during the HAp precipitation approach. The prepared HAp/NCh materials were characterised with Fourier-transform infrared spectroscopy, thermogravimetric analysis, X-ray diffraction, and energy-dispersive X-ray spectroscopy. The surface of prepared specimens was observed using scanning electron microscopy. The presence of nanofibres was confirmed by non-invasive backscattering with dynamic light scattering particle size analysis. Moreover, the synergic effect of chitin nanofibres on the mechanical resistance of HAp-based composite was investigated. The sample with 5% of chitin nanofibres exhibited about 10 times higher compression strength than the pure HAp. All these results essentially indicate that the prepared material can be a potential candidate for bone tissue engineering applications and further development.

Keywords: *hydroxyapatite, nanochitin, biocomposites*

Received: 25.02.2022
Accepted: 21.06.2022

1. Introduction

Despite the rapid development of regenerative medicine, large tissue damage caused by diseases or life-threatening accidents cannot be restored by the organism itself. Indeed, the extensiveness of these defects means that they are irreversible. Bone is the most mineralised tissue in vertebrates, often exposed to many risks of damage. From an anatomical point of view, it is a composite material composed of mineralised protein fibrils (i.e., collagen type I) with a high organisation level [1, 2]. The combination of the mineral phase and proteins means bones are simultaneously flexible and stiff. Almost 70% of their content is inorganic [3] – mainly calcium phosphates [4] and calcium carbonates [5]. Based on the porosity and mechanical properties, bone can be divided into two types, more porous trabecular (spongy) bone and cortical bone with lower porosity and higher mechanical resistance [5]. The repair of critical bone defects which occur after accidents, infections, osteoporosis, or cancer resections is a clinical challenge due to the apparent inability of hard tissue to fully self-heal [6, 7]. Therefore, functional biomaterials seem to be a promising solution to solve bone repairing problems. Among various materials used for hard tissue regeneration, hydroxyapatite (HAp, with the chemical formula $Ca_{10}(PO_4)_6(OH)_2$) and its derivatives are especially interesting [8]. Their outstanding biocompatibility and unique bioactivity allow them to be permanently incorporated into bone substitute materials [9, 10]. HAp in its pure form is distinguished by its non-inflammatory, non-toxic [11], and osteoconductive properties [6], and it possesses the ability to create chemical bonds with natural tissue [4, 12]. Nevertheless, the use of pure HAp is limited due to the occurrence of brittle fractures of synthetically produced material [4]. Therefore, HAp is commonly used as a composite component or as a thin layer, improving the biocompatibility of implants. For example, Rogina *et al.* [2] prepared a composite based on HAp/polycaprolactone/poly(lactic acid) to improve the brittleness and poor load bearing of HAp. The low stiffness of the HAp scaffold was improved by a thin polycaprolactone/poly(lactic acid) coating, resulting in the almost 18-fold increase in Young's modulus. Kim *et al.* [13] developed HAp nanopowder/chitosan composite scaffolds with high strength and controlled pore structures. Moreover, the authors cultivated mouse pre-osteoblastic cells (MC3T3-E1) on prepared scaffolds and observed higher differentiation and mineralisation in samples with higher HAp content. Other examples of synthetic and natural polymers used for HAp composite reinforcement are poly(glycolic acid) (PGA) [14], collagen [1, 3, 15], and chitin and their derivatives [6, 11, 12, 16-19]. The great potential of natural materials and their easy availability have prompted their functionalisation and further development.

Chitin is the second most widespread polysaccharide (after cellulose) worldwide, with an annual production by marine organisms of 1×10^{12} to 1×10^{14} tons [20]. From a structural point of view, this biopolymer is composed of *N*-acetyl-D-glucosamine units linked by β-(1,4) glycosidic bonds [21]. However, commercially available material is more like a copolymer of *N*-acetylglucosamine and glucosamine units, due to alkaline treatment during isolation [22]. Chitin biosynthesis takes place in many living organisms, from very simple organisms such as fungi, sponges, and diatoms, to more advanced organisms like insects, spiders, crustaceans, and others [23, 24]. In its native form, chitin acts as functional and structural component in exo- and endoskeletons [25]. Chitin has a natural tendency to organise into fibrils (also known as rods or crystallites) of ~3 nm in diameter, which are stabilised by intermolecular hydrogen bonds formed between the amine and carbonyl groups. Its peritrophic matrix fibrils can reach 0.5 μm in length and are frequently grouped in bundles containing parallel groups of ≥10 single fibrils [26]. Due to the differences in biopolymeric chain arrangement, three allomorphic forms of chitin designated as α, β, and γ can be distinguished [27, 28]. In β-chitin, the conterminous layers are parallel and go

in the same direction, providing them with the most flexible structures of all allomorphs [28, 29]. These polymorphs do not have inter-sheet hydrogen bonds along the b axis, in contrast to α-form. This fact makes β-chitin more vulnerable to intracrystalline swelling of polar guest molecules (like water, alcohols, and amines) [25] and, consequently, ensures easier processability. Chitin plays a crucial role as an integral part of the exoskeletons of invertebrates and as crystal-directing templates during biomineralisation [30]. The natural tendency of chitin to interact with minerals makes them an exciting candidate to prepare organic-inorganic composites [16]. The fundamental discovery of Iijima and Moriwaki [31] has shown a relationship between apatite and β-chitin in the natural shell of the marine mollusc *Lingula unguis*. This discovery strongly indicates that the chitinous matrix has a massive impact on apatite crystal formation and orientation.

In this study, we have focussed on designing a novel HAp/β-chitin biocomposite. For the first time, β-chitin nanofibres obtained from *Sepia officinalis* cuttlebone have been used as reinforcement for HAp synthesised by precipitation with sodium citrate. The crucial part of the work was the physicochemical characterisation of obtained materials and the determination of the synergistic effect of chitin on the mechanical resistance of created materials. Furthermore, the effect of synthesis parameters on HAp/NCh properties as the chitin content or HAp maturation time have been developed here. The obtained results clearly show the great application potential of chitin nanofibre reinforcement.

2. Materials and methods

2.1. Preparation of the β-Chitin Nanofibres

For nanofibre preparation, dry *S. officinalis* cuttlebone was used as raw material and processed according to the modified procedure described previously [32]. The preparation began by crushing the material into small particles (1-2 cm) and then immersing it in 3 M CH_3COOH (Chempur, Poland) to remove calcium carbonate and other minerals (see Figure 1). The demineralisation process was carried out for 3 days at room temperature until minerals had been eliminated. After that, the organic residue was neutralised in deionised water and transferred to 2.5 M NaOH (Chempur, Poland) solution for protein removal. Similarly to the first step, deproteinisation was carried out at room temperature for 3 days. Then, chitinous sheets were carefully moved and washed with deionised water until the effluent had reached a neutral pH. To fabricate the β-chitin nanofibrils, 8.33 g of wet pure chitinous sheets was mixed with 200 ml ultrapure distilled water titrated by and 3 M HCl to pH 3 (about 125 µl). Then, ultrasonic treatment was carried out in an ice/water bath for 4 h with shaking every 20 min. Sonication was performed at 60 kHz with a Sonic-3 (Polsonic, Poland). After the process, the homogeneous solution was filtered through a fine sieve and then centrifuged (5000 rpm, 5 min) for nanochitin (NCh) isolation. The dry chitin content in the prepared hydrogel was determined to be ~1%. Finally, the solution was filtered using paper filter with a grate of 11 µm.

2.2. Synthesis of HAp/NCh Composite via Precipitation

HAp/NCh biocomposites were synthesised with a modified precipitation method described previously [33]. Two solutions (1:1 v/v, 50 ml each) were prepared. (I) 0.1 M calcium chloride dihydrate ($CaCl_2 \cdot 2H_2O$) (Sigma Aldrich, USA) + 0.4 M sodium citrate tribasic dihydrate ($Na_3(Cit) \cdot 2H_2O$) (Sigma Aldrich, USA) + x chitin nanofibre dispersion (x = 10, 30, or 50 ml) and (II) 0.12 M sodium phosphate dibasic ($NaHPO_4$) (Chempur, Poland) were mixed at room temperature. Moreover, a pure HAp reference sample was prepared (x = 0). The pH of the mixture was titrated to 8.5 using 0.1 M NaOH. Then, the mixtures were incubated in a 250 ml Erlenmeyer flask, sealed with a rubber stopper, and incubated with mixing (80 rpm) using an IKA KS 4000i control incubator (Ika Werke

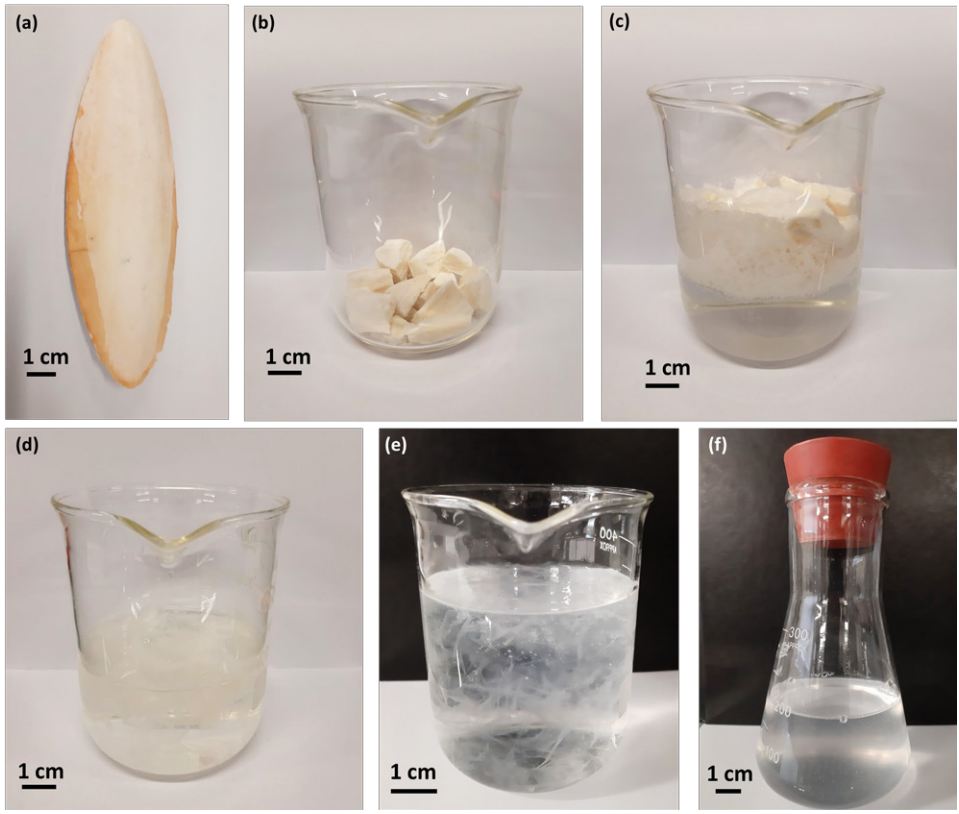

Figure 1. Schematic view of β-chitin nanofibril preparation. The photographs show *Sepia officinalis* cuttlebone used in this study (a), cuttlebone after crushing (b), small pieces of cuttlebone during demineralisation (c), demineralised cuttlebone during deproteinisation (d), β-chitin sheets obtained after the isolation process (e), and β-chitin nanofibril hydrogel after ultrasonication (f).

GmbH, Germany) at 80°C. The precipitates were allowed to mature for 6 h (Sample HAp/NCh_6, x = 10 ml of the chitin), 24 h (HAp/NCh_24, x = 30 ml of the chitin), or 96 h (HAp/NCh_96, x = 50 ml of the chitin). After that, the prepared biocomposites were centrifuged (4000 rpm, 10 min) using a 5810 R centrifuge (Eppendorf, Germany) and washed with distilled water. Finally, the samples were dried in cubic forms in convectional dryer at 40°C for 24 h. The final chitin nanofibre content in prepared samples (v/v) was: HAp/NCh_6, 1% chitin, HAp/NCh_24, 2.5% chitin, and HAp/NCh_96, 5% chitin.

2.3. Characterisation Techniques

The differences in the chemical composition of obtained specimens were analysed by attenuated total reflectance Fourier-transform infrared (ATR-FTIR) spectroscopy using a VERTEX 70 spectrometer (Bruker, Germany). The investigation was performed over a wide wavenumber range of 4000-400 cm^{-1} (resolution of 0.5 cm^{-1}). The degree of acetylation (DA) – Equation (1) – and the degree of deacetylation (DD) – Equation (2) – were calculated for the isolated chitin [34]:

$$DA\% = [(A_{1640}/A_{3392}) \times 100\%)]/1.33 \quad (1)$$

$$DD\% = 100\% - DA\% \quad (2)$$

where A_{1640} and A_{3392} correspond to the absorbance for amide I and OH vibrations, respectively.

The qualitative characterisation of the samples observed during heating was performed by thermogravimetric analysis (TGA) using a Jupiter STA 449 F3 instrument (Netzsch GmbH, Germany). Samples weighing approximately 10 mg were placed in an Al_2O_3 thermobalance and heated from 30 to 1000°C (heating rate 10°C/min) in a nitrogen atmosphere. Additionally, a derivative thermogravimetric (DTG) curve was prepared.

The size of dispersed chitin nanofibres was determined by a Zetasizer Nano ZS instrument (Malvern Instruments Ltd., Malvern, UK) using non-invasive backscattering (NIBS) with dynamic light scattering (DLS). Ultrapure deionised water was used as solvent and the results show particles with a content >1%.

The synthesised composite's structure was investigated by X-ray diffraction (XRD) (Panalytical, Empyrean model, Almelo, the Netherlands) with a copper anode (CuKα, λ = 1.54 Å). Measurements for each sample were conducted at set parameters: voltage 45 kV, anode current 40 mA, and scanning range 30-120°. The peaks were analysed using HighScore Plus together with ICDD-JCPDS crystallographic database.

The surface morphology and microstructure were observed by scanning electron microscopy (SEM). Micrographs were collected with an EVO 40 scanning electron microscope (Carl Zeiss AG, Germany) with EDS Ultim Max 65 (Oxford Instruments, High Wycombe, UK). Before analysis, the samples were coated with a thin Au layer.

The mechanical properties of prepared materials were determined by a compressive test. The static compression test was carried out until 20% relative sample reduction or sample destruction manifested by a sudden decrease in the strength (brittle cracking). Specimens were prepared with a cylinder prism with a diameter of ca. 4 mm and a thickness of ca. 6 mm. The parameters of analysis were: desired compression 0.1 MPa and rate of compression (constant beam falling) 0.5 mm/min. The analysis was performed with a Z020 apparatus (Zwick/Roell, Poland). The compressive strength was examined by a dry test and determined by the highest obtained stress during a static compression test. The error value was calculated in each experiment based on the mean and standard deviation from three measurements.

3. Results and Discussion

One of the purposes of this article was to evaluate the morphological and physicochemical properties of prepared HAp/NCh biocomposites. Thus, SEM with energy-dispersive X-ray spectroscopy (EDS) was used (Figure 2). The HAp/NCh_6 sample, with a lower chitin content (1%) and a shorter maturation time (6 h), formed aggregates with an average diameter close to 1 μm. The material comprises non-uniform particles with a sharp (plate-like) texture. The sample with a higher chitin nanofibre content (HAp/NCh_24) presented a similar morphology. However, the diameter of the average aggregates increased slightly, probably due to the longer maturation time (24 h). The HAp/NCh_96 sample, with a higher chitin content (5%) and the longest maturation time (96 h), presented marked differences. It has a uniform, smooth, and dense surface. The material seems to be combined into a single unit. Similar flat and dense surface morphology has been previously described by Supelano *et al.* [14] for a HAp/chitosan composite. The EDS elemental analysis revealed

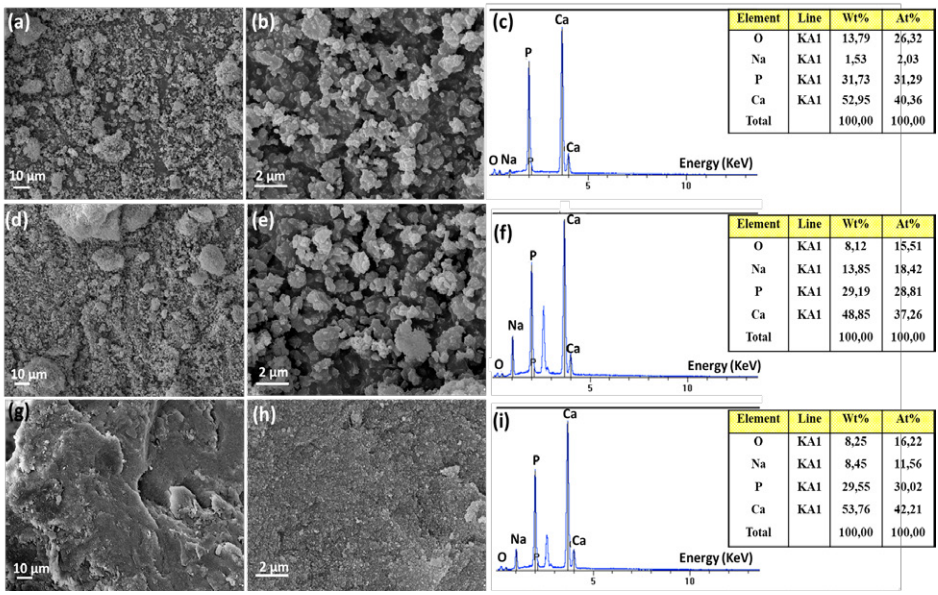

Figure 2. Scanning electron micrographs of HAp/NCh_6 (a and b) and energy-dispersive X-ray spectra of the sample (c). Scanning electron micrographs of HAp/NCh_24 (d and e) and energy-dispersive X-ray of the sample (f). Scanning electron micrographs of HAp/NCh_96 (g and h) and energy-dispersive X-ray of the sample (i).

a calcium-to-phosphate ratio (Ca/P) in HAp/NCh_6 and HAp/NCh_24 of 1.67, which is analogous to the HAp ratio in mature human hard tissue [11, 35]. However, the final Ca/P ratio of HAp/NCh_96 was higher (1.81).

To confirm the presence of nano-sized chitin dispersion, the prepared biopolymer was characterised by NIBS-DLS particle size analysis (Figure 3). The material comprises two fundamental size dimensions. Therefore, we can assume that that the material is some kind of fibre. The smaller values are between 45 and 105 nm and probably correspond to the diameter of chitinous nanofibre groups (from 15 to 30 fibres of 3 nm). There are also broad bands of larger particles of 650-1100 nm. These values may correlate with the length of the prepared nanofibres [32]. The results confirmed the presence of nanoparticles because a minimum of one dimension is within 100 nm. However, the randomness of fibre arrangement in the dispersion during the reflection also resulted in larger values. Nevertheless, the presence of particle fractions with a size close to 1 µm indicates incomplete nanofibrilaton of isolated chitin.

ATR-FTIR analysis was used to determine the presence of distinct functional groups and to investigate potential interactions between both phases (Figure 4). The most intense band observed for pure HAp with a maximum close to 1020 cm^{-1} unambiguously corresponds to νPO_4^{3-}. Another HAp signal occurs at 559 cm^{-1}, associated with stretching and bending vibrations of the phosphate group [11, 36]. The spectra recorded for pure NCh show a wide band with two narrow peak ranges of 3600-3200 cm^{-1}. As described previously, it could be related to stretching vibrations of hydroxyl groups [11, 37]. C-H stretching vibrations occur at 2844 cm^{-1} [27]. There are characteristic signals for β-chitin signals including amide I (intermolecular [C=O···H-N] and intramolecular [C=O···HO(C6); C=O···HN] hydrogen bonds) and amide II (νN-H and νC-N) at 1640

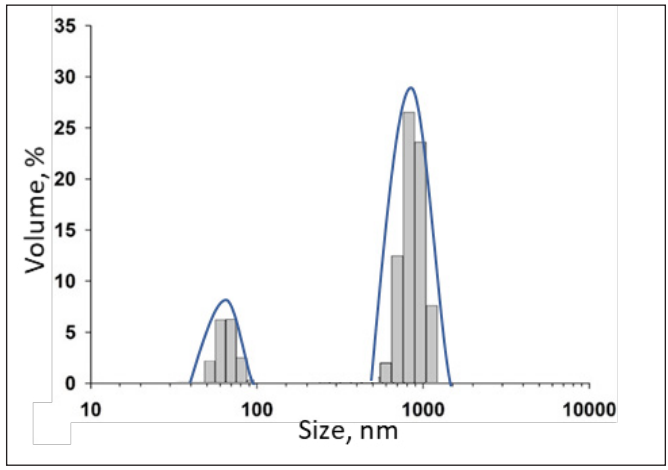

Figure 3. Size distributions of prepared chitinous nanofibre dispersion.

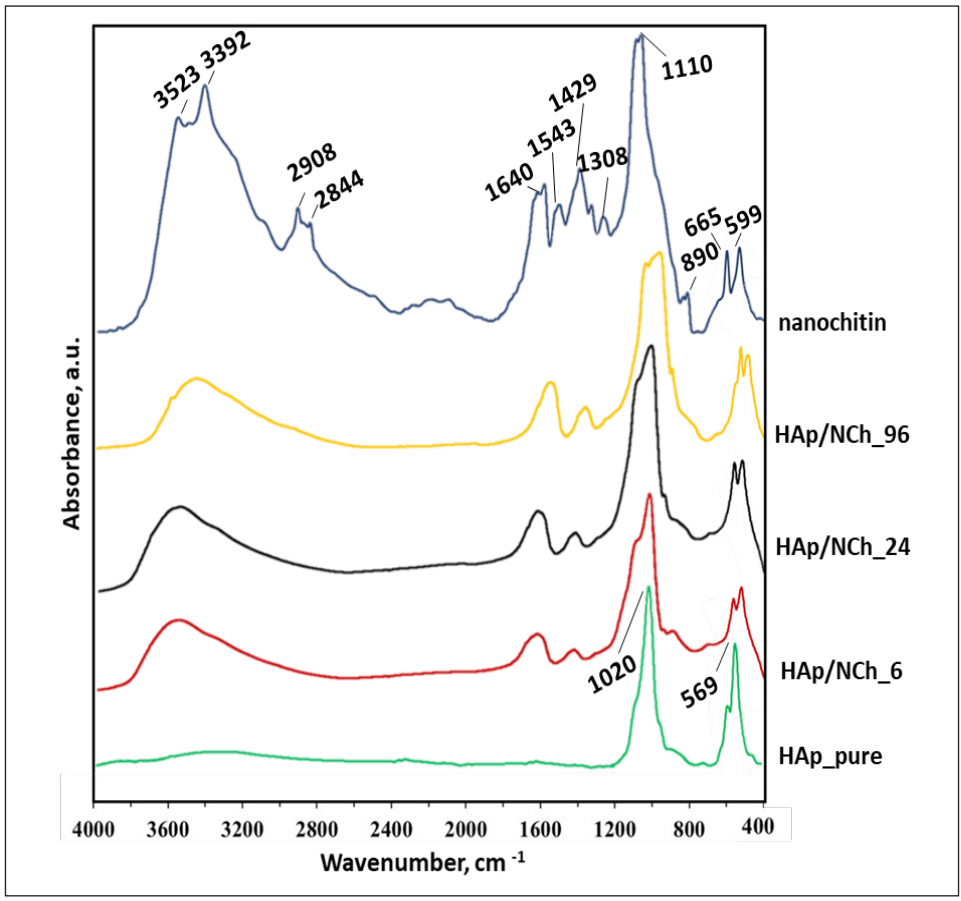

Figure 4. Attenuated total reflectance Fourier-transform infrared spectra of prepared specimens and pure components.

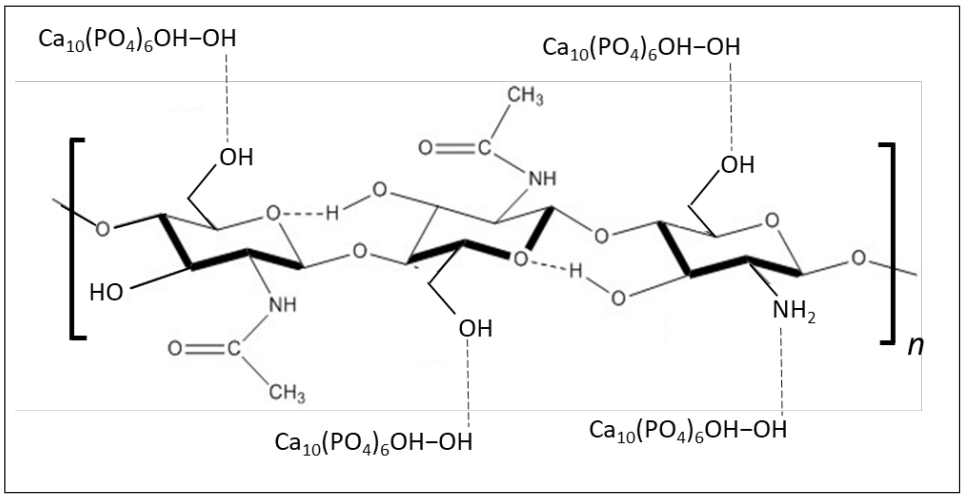

Figure 5. Schematic representation of possible physical interactions between hydroxyapatite and partially deacetylated chitin.

and 1543 cm^{-1}, respectively [28]. Next, there is a narrow peak around 1430 cm^{-1} associated with $-CH_3$ and $-CH_2$ in-plane deformation [11]. Amide III (νC-N and δN-H) occurs at 1308 cm^{-1}. Moreover, there is a characteristic band for β-chitin with a partially divided peak associated with C-O stretching vibrations around 1110 cm^{-1}. Further analysis revealed the typical polysaccharide β-glycosidic bond signal at 890 cm^{-1} [38-40] and a fingerprint region below 700 cm^{-1} [41]. The DA of prepared chitin was estimated as 69%; thus, the DD was 31%. Gbenebor *et al.* [34] reported similar values for shrimp-based chitin isolated by alkaline treatment. In the case of prepared biocomposites, the signals from both phases can be found. The broad, smooth peaks with a maximum at 3450-3400 cm^{-1} suggest hydrogen interaction between HAp and NCh fibres (see Figure 5). Moreover, there are very interesting signals for prepared materials in the region of amide I and amide II of chitin. These signals suggest that HAp nanoparticles may interact with the $-NH_2$ groups of partially deacetylated chitin via hydrogen bonds [42]. There are other intriguing signals for the HAp region, as determined by the HAP/NCh sample spectra shifting from 1020 cm^{-1} to lower values. Kin *et al.* [13] explained this phenomenon as potential ionic interactions between C-O-C and Ca^{2+}. However, the absence of new absorption bands may indicate solely physical interactions between chitin nanofibres and HAp [2].

The thermal stability of the prepared materials was determined by TGA (Figure 6). The first decrease in sample mass began at around 100°C, which is related to moisture removal from the surface and pores [11, 43, 44]. The loss of physically and chemically connected water molecules ranged from 3% to 7%. The second visible decrease in sample mass occurred at 300-450°C. These regions correspond to thermal and oxidative decomposition of glycosidic bonds of chitin [43], which is consistent with the graph shown in Figure 4d (pure chitin). The curves also highlight the dependence between the NCh content and the second visible decrease in mass. The final mass loss occurred at >700°C for all prepared biocomposites and indicates the dehydroxylation stage and decomposition of HAp [44]. As expected, the sample containing the highest chitin content (HAp/NCh_96) showed lower thermostability with a total mass loss of 18%. In comparison, the sample with the lowest chitin content (HAp/NCh_6) showed 15% mass loss.

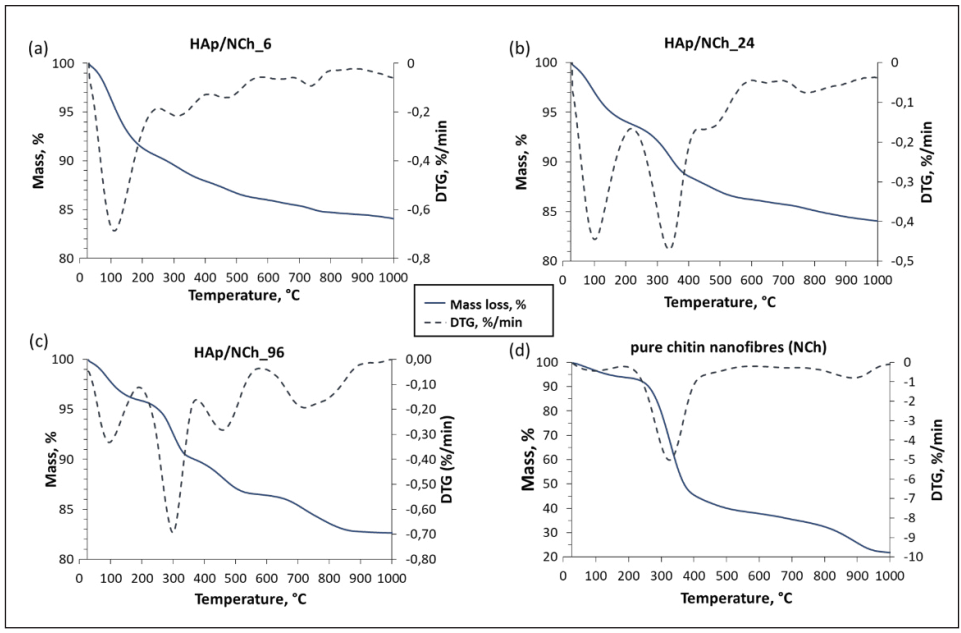

Figure 6. Derivative thermogravimetric curves showing the results of thermogravimetric analysis of the prepared biocomposites and pure chitin nanofibres as a reference.

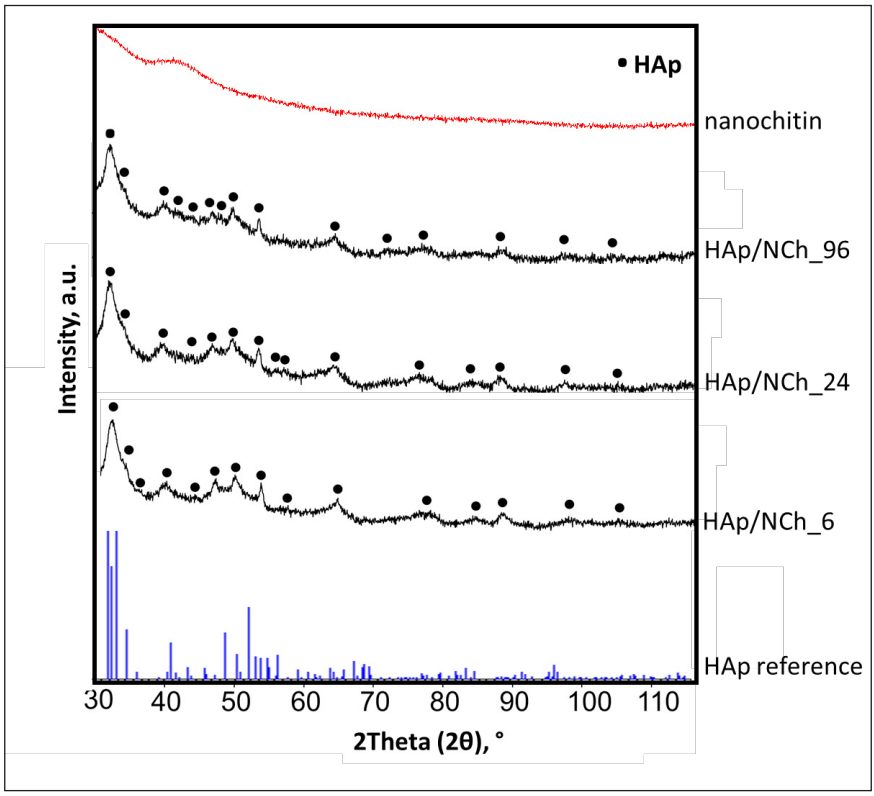

Figure 7. X-ray diffraction patterns of prepared materials and reference samples.

The crystalline structures of the prepared biocomposites as well as pure components (HAp and chitin nanofibres) were investigated with XRD analysis and are shown in Figure 7. The diffraction peaks at 2θ = 32.2°, 39.8°, 41.0°, 42.4°, 44.5°, 46.7°, 49.6°, 53.4°, and 63.4° correspond to the crystallographic lattice planes: (002), (112), (130), (103), (302), (400), (222), (213), (004), (150) of HAp (JCPDS No: 01-075-9526), respectively. As expected, samples of the biocomposite with a longer maturation time showed higher crystallinity because of the greater number of diffraction peaks. Thus, NCh can influence the crystallinity of the HAp, making it more grain-refined. Evidence of the presence of chitin in the tested samples was hampered considering that the diffraction angles for chitin are usually observed at 2θ = 9.3° and 19.3° (unpublished data) [36]. However, the diffractograms of the biocomposites clearly differ from the reference material.

As shown in Figure 8, the compressive strength of all samples increased as the chitin content increased. Pure HAp had a mean compressive strength of 12 MPa. Mechanical resistance for compression increased slightly to 13 and 18 MPa for HAp/NCh_6 and HAp/NCh_24, respectively. However, there was a significant increase in mechanical resistance (compressive strength) for the sample with 5% chitin increased to 117 MPa. Indeed, HAp/NCh_96 exhibited about 10-times higher mechanical properties than pure HAp. These results confirmed the synergic effect of the interaction between HAp and chitin nanofibres. Reinforcement of nanofibres probably allowed avoiding the brittle cracking of HAp due to good dispersion of the inorganic phase. In comparison, native cortical bone tissue has shown compressive strength at a value range of 100-230 MPa [5]. Previously, Chang *et al.* [36] fabricated chitin/HAp hydrogels with weaker mechanical properties, where compressive strength was estimated at 200-240 kPa.

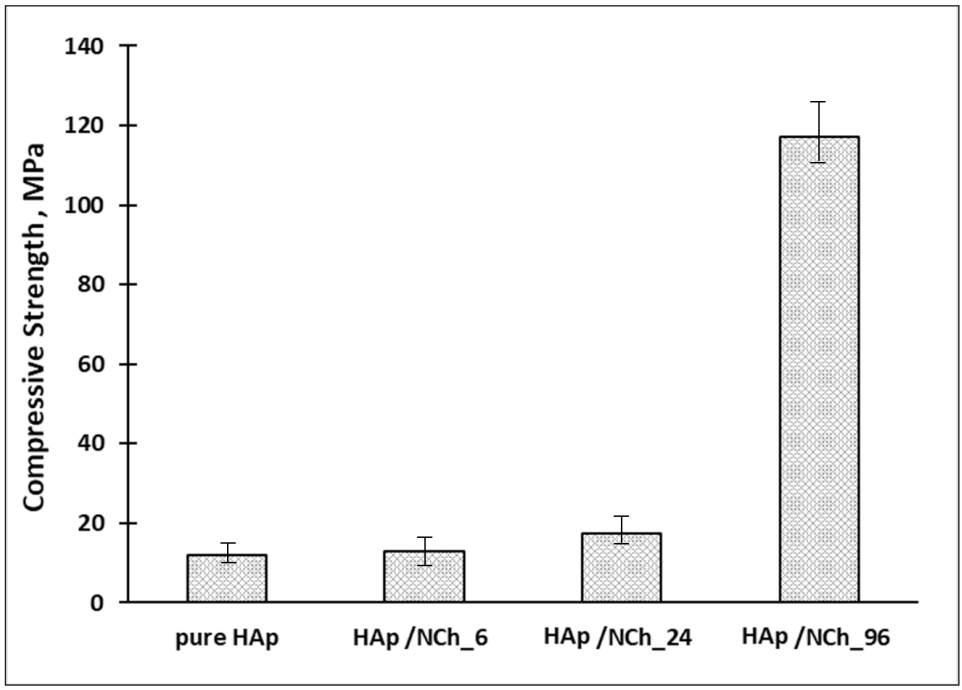

Figure 8. Results of compressive strength test for the obtained materials and reference hydroxyapatite (HAp).

4. Conclusion

We have presented a novel approach for the application of β-chitin nanofibres as reinforcement for HAp-based composites. Our analyses confirmed the presence of chitin nanofibres, with the minimum chitin fibre diameter estimated at 45 nm. Scanning electron micrographs support the conclusion that the composite components are strongly interconnected. EDS analysis showed that two of the prepared materials achieved a Ca/P ratio of 1.67, the same as natural bone tissue. The FTIR spectra confirmed the presence of β-chitin and HAp as well as physical interaction between both phases by the shift in the most characteristic bands (hydrogen bonds). TGA/DTG showed that the prepared composite is thermally stable up to about 150°C. As expected, samples containing the highest chitin content displayed lower thermostability. XRD analysis confirmed the presence of HAp in crystalline form. The longer maturation time led to greater crystallinity. Finally, a study of mechanical properties of prepared material showed that 5% chitin in the prepared material allows for an almost 10-fold increase in compression strength.

5. Acknowledgements

This work was partially supported by the Polish Ministry of Education and Science.

6. References

[1] Delgado-López JM, Bertolotti F, Lyngsø J, Pedersen JS, Cervellino A, Masciocchi N, Guagliardi A; (2017) The synergic role of collagen and citrate in stabilizing amorphous calcium phosphate precursors with platy morphology. Acta Biomater 49, 555-562.

[2] Rogina A, Antunovic M, Milovac D; (2019) Biomimetic design of bone substitutes based on cuttlefish bone-derived hydroxyapatite and biodegradable polymers. J Biomed Mater Res Part B 107B, 197-204

[3] Tampieri A, Celotti G, Landi E, Sandri M, Roveri N, Falini G; (2002) Biologically inspired synthesis of bone-like composite : self-assembled collagen fibers/ hydroxyapatite nanocrystals. J Biomed Mater Res Part A 67, 618-625.

[4] Sobczak A, Kowalski Z; (2007) Materiały hydroksyapatytowe stosowane w implantologii. Czas Tech 1, 149-158.

[5] Donnaloja F, Jacchetti E, Soncini M, Raimondi MT; (2020) Natural and synthetic polymers for bone scaffolds optimization. Polymers 12, 905.

[6] Duan B, Shou K, Su X, Niu Y, Zheng G, Huang Y, Yu A, Zhang Y, Xia H, Zhang L; (2017) Hierarchical microspheres constructed from chitin nanofibers penetrated hydroxyapatite crystals for bone regeneration. Biomacromolecules 18, 2080-2089.

[7] Sözen T, Özışık L, Başaran NÇ; (2017) An overview and management of osteoporosis. Eur J Rheumatol 4, 46-56.

[8] Molino G, Palmieri MC, Montalbano G, Fiorilli S, Vitale-Brovarone C; (2020) Biomimetic and mesoporous nano-hydroxyapatite for bone tissue application: a short review. Biomed Mater 15, 022001.

[9] Jaroszewicz J, Idaszek J, Choinska E, Szlazak K, Hyc A, Osiecka-Iwan A, Swieszkowski W, Moskalewski S; (2019) Formation of calcium phosphate coatings within polycaprolactone scaffolds by simple, alkaline phosphatase based method. Mater Sci Eng C 96, 319-328.

[10] Pina S, Oliveira JM, Reis RL.; (2015) Natural-based nanocomposites for bone tissue engineering and regenerative medicine: a review. Adv Funct Mater 27, 1143-1169.

[11] Szatkowski T, Kołodziejczak-Radzimska A, Zdarta J, Szwarc-Rzepka K, Paukszta D, Wysokowski M, Ehrlich H, Jesionowski T; (2015) Synthesis and characterization of hydroxyapatite/chitosan composites. Physicochem Probl Miner Process 51, 575-585.

[12] Chen P, Liu L, Pan J, Mei J, Li C, Zheng Y; (2019) Biomimetic composite scaffold of hydroxyapatite/gelatin-chitosan core-shell nano fibers for bone tissue engineering. Mater Sci Eng C 97, 325-335.
[13] Kim H, Jung G, Yoon J, Han J, Park Y, Kim D, Zhang M, Kim D; (2015) Preparation and characterization of nano-sized hydroxyapatite/alginate/chitosan composite scaffolds for bone tissue engineering. Mater Sci Eng C 54, 20-25.
[14] Supelano NM, Amador AS, Duran HE, Ballesteros DP; (2018) Dielectric properties of PLA-PGA-chitosan - hydroxyapatite composites. J Mater Environ Sci 9, 2956-2963.
[15] Ehrlich H, Douglas T, Scharnweber D, Hanke T, Born R, Bierbaum S, Worch H; (2005) Hydroxyapatite crystal growth on modified collagen I-templates in a model dual membrane diffusion system. Zeitschrift Anorg Allg Chemie 631, 1825-1830.
[16] Kawata M, Azuma K, Izawa H, Morimoto M, Saimoto H, Ifuku S; (2016) Biomineralization of calcium phosphate crystals on chitin nanofiber hydrogel for bone regeneration material. Carbohydr Polym 136, 964-969.
[17] Madhumathi K, Binulal NS, Nagahama H, Tamura H, Shalumon KT, Selvamurugan N, Nair SV, Jayakumar R; (2009) Preparation and characterization of novel β-chitin-hydroxyapatite composite membranes for tissue engineering applications. Int J Biol Macromol 44, 1-5.
[18] Sudheesh Kumar PT, Srinivasan S, Lakshmanan VK, Tamura H, Nair SV, Jayakumar R; (2011) β-Chitin hydrogel/nano hydroxyapatite composite scaffolds for tissue engineering applications. Carbohydr Polym 85, 584-591.
[19] Ehrlich H, Krajewska B, Hanke T, Born R, Heinemann S, Knieb C, Worch H; (2006) Chitosan membrane as a template for hydroxyapatite crystal growth in a model dual membrane diffusion system. J Memb Sci 273, 124-128.
[20] Yadav M, Goswami P, Paritosh K, Kumar M, Pareek N, Vivekanand V; (2019) Seafood waste: a source for preparation of commercially employable chitin/chitosan materials. Bioresour Bioprocess 6, 8.
[21] Rameshthangam P, Solairaj D, Arunachalam G, Ramasamy P; (2018) Chitin and chitinases: biomedical and environmental applications of chitin and its derivatives. J Enzym 1, 20-43.
[22] Pillai CKS, Paul W, Sharma CP; (2009) Chitin and chitosan polymers: chemistry, solubility and fiber formation. Prog Polym Sci 34, 641-678.
[23] Duan B, Huang Y, Lu A, Zhang L; (2018) Recent advances in chitin-based materials constructed via physical methods. Prog Polym Sci 82, 1-33.
[24] Machałowski T, Amemiya C, Jesionowski T; (2020) Chitin of Araneae origin: structural features and biomimetic applications: a review. Appl Phys A 126, 678.
[25] Younes I, Rinaudo M; (2015) Chitin and chitosan preparation from marine sources Structure, properties and applications. Mar Drugs 13, 1133-1174.
[26] Merzendorfer H, Zimoch L; (2003) Chitin metabolism in insects: structure, function and regulation of chitin synthases and chitinases. J Exp Biol 206, 4393-4412.
[27] Focher B; (1992) Structural differences between chitin polymorphs and their precipitates from solutions - evidence from CP-MAS 13 C -NMR, FT-IR and FT-Raman spectroscopy. Carbohydr Polym 17, 97-102.
[28] Kaya M, Mujtaba M, Ehrlich H, Salaberria AM, Baran T, Amemiya CT, Galli R, Akyuz L, Sargin I, Labidi J; (2017) On chemistry of γ-chitin. Carbohydr Polym 176, 177-186.
[29] Ehrlich H; (2010) Chitin and collagen as universal and alternative templates in biomineralization. Int Geol Rev 52, 661-699.

[30] Ehrlich H; (2013) Biomimetic potential of chitin-based composite biomaterials of poriferan origin, in: Ruys AJ (Ed), Biomimetic biomaterials: structure and applications. Woodhead Publishing, Cambridge, 46-66.
[31] Iijima M, Moriwaki Y; (1990) Orientation of apatite and organic matrix in *Lingula unguis* shell. Calcif Tissue Int 47, 237-242.
[32] Fan Y, Saito T, Isogai A; (2008) Preparation of chitin nanofibers from squid Pen β-chitin by simple mechanical treatment under acid conditions. Biomacromolecules 9, 1919-1923.
[33] Delgado-López JM, Frison R, Cervellino A, Gómez-Morales J, Guagliardi A, Masciocchi N; (2013) Crystal size, morphology, and growth mechanism in bio-inspired apatite nanocrystals. Adv Funct Mater 24, 1090-1099.
[34] Gbenebor OP, Adeosun SO, Lawal GI, Jun S, Olaleye SA; (2017) Acetylation, crystalline and morphological properties of structural polysaccharide from shrimp exoskeleton. Eng Sci Technol 20, 1155-1165.
[35] Mahamid J, Sharir A, Gur D, Zelzer E, Addadi L, Weiner S; (2011) Bone mineralization proceeds through intracellular calcium phosphate loaded vesicles: a cryo-electron microscopy study. J Struct Biol 174, 527-535.
[36] Chang C, Peng N, He M, Teramoto Y, Nishio Y, Zhang L; (2013) Fabrication and properties of chitin/hydroxyapatite hybrid hydrogels as scaffold nano-materials. Carbohydr Polym 91, 7-13.
[37] Kumirska J, Czerwicka M, Kaczyński Z, Bychowska A, Brzozowski K, Thöming J, Stepnowski P; (2010) Application of spectroscopic methods for structural analysis of chitin and chitosan. Mar Drugs 8, 1567-1636.
[38] Focher B, Naggi A, Torri G, Cossani A, Terbojevich M; (1992) Structural differences between chitin polymorphs and their precipitates from solutions - evidence from CP-MAS 13C NMR, FT-IR and FT-Raman spectroscopy. Carbohydr Polym 17, 97-102.
[39] Machałowski T, Idaszek J, Chlanda A, Heljak M, Piasecki A, Swięszkowski W, Jesionowski T; (2022) Naturally prefabricated 3D chitinous skeletal scaffold of marine demosponge origin, biomineralized *ex vivo* as a functional biomaterial. Carbohydr Polym 275, 118750.
[40] Machałowski T, Rusak A, Wiatrak B, Haczkiewicz-Leśniak K, Popie A, Jaroszewicz J, Żak A, Podhorska-Okołów M, Jesionowski T; (2021) Naturally formed chitinous skeleton isolated from the marine demosponge *Aplysina fistularis* as a 3D scaffold for tissue engineering. Materials 14, 2992.
[41] Ogawa Y, Kimura S, Saito Y, Wada M; (2012) Infrared study on deuteration of highly-crystalline chitin. Carbohydr Polym 90, 650-657.
[42] Wysokowski M, Motylenko M, Stöcker H, Bazhenov VV, Langer E, Dobrowolska A, Czaczyk K, Galliet R; (2013) An extreme biomimetic approach: hydrothermal synthesis of β-chitin/ZnO nanostructured composites. J Mater Chem B. 1, 6469-6476.
[43] Chang C, Peng N, He M, Teramoto Y, Nishio Y, Zhang L; (2013) Fabrication and properties of chitin/hydroxyapatite hybrid hydrogels as scaffold. Carbohydr Polym 91, 7-13.
[44] Wang T, Dorner-Reisel A, Mu E; (2004) Thermogravimetric and thermokinetic investigation of the dehydroxylation of a hydroxyapatite powder. J Eur Cer Soc 24, 693-698.